Assembly Strategies for Chamferless Parts

Michael E. Caine, Tomás Lozano-Pérez, Warren P. Seering

Artificial Intelligence Laboratory
Massachusetts Institute of Technology
Cambridge, MA 02139

Abstract

The reliability of assembly strategies is inherently constrained by various forms of uncertainty. Such uncertainty results from an imperfect knowledge of the parts being assembled, as well as performance limitations of the devices performing the assembly. To develop reliable assembly strategies it is necessary to consider a priori the effects of such uncertainty. In this paper we illustrate the need for planning in assembly and describe a set of modelling and planning techniques developed to generate robust force control strategies for a certain class of assemblies. Specifically, we develop strategies for the chamferless insertion of a planar peg into a hole and the insertion of a three dimensional rectangular peg into a rectangular hole. The complexity of applying these techniques in three dimensions is also discussed.

Introduction

A great deal of analysis has been done on the insertion of a cylindrical peg into a chamfered hole in the past several years [3, 6, 7, 8]. For this task, implementations of assembly strategies based on the specification of a passive compliance have been developed [7, 8]. Devices incorporating these strategies, such as the Remote Center Compliance (RCC), require no a priori specification of the contact configurations through which the parts must pass during assembly. In this paper we examine cases where such strategies are not sufficient to guarantee assembly. In particular, we examine the chamferless insertion of a planar peg into a hole, and the chamferless insertion of a three dimensional rectangular peg into a hole. For these cases we develop strategies that guarantee successful assembly by constraining the allowable contact configurations between the parts in order to avoid configurations that will cause the assembly to fail,

The development of the RCC resulted from a planar analysis of the force interactions between the peg and the hole [8]. Extensions of this kind of analysis to other classes of insertions, specifically parts that lack rotational symmetry about their major axis, have also been performed [1, 6]. However, these approaches do not directly consider the effects of uncertainty on the reliability of the resulting assembly strategies. The dependence of these strategies on the accuracy of modeled parameters, sensor information, and positioning devices reduces the likelihood that such strategies may be implemented reliably.

General techniques for synthesizing assembly strategies that take uncertainty into account directly have been developed [2, 4]. The difficulty of using such techniques with actual physical systems of even moderate complexity have limited their application. One means of overcoming the difficulties posed by real-world complexity is to limit the generality of such approaches by considering simplifications applicable to specific classes of assembly that are of particular interest. The resulting strategies, including the ones described in this paper, have proved to be useful despite being limited to a narrow class of assemblies.

The RCC

In describing the analysis underlying the design of the RCC, Whitney defines four distinct stages of assembly for the peg and hole: approach, chamfer crossing, one-point contact, and two-point contact [8]. The last three stages involve contact between the peg and hole and therefore give rise to contact forces between them. In the analysis of these contact stages, the static force and moment equilibrium conditions for the peg are determined and expressed in terms of the geometry of the peg and hole and the coefficient of friction.

To illustrate the nature of the contact forces between the peg and hole, Whitney represented graphically the linearized force-moment equilibrium expressions in a two dimensional space as shown in Figure 1. The external forces are assumed to be applied to the tip of the peg as shown, and the term λ is defined to be $\lambda = \frac{l}{2r\mu}$ where r is the radius of the peg and l is the depth to which the peg is inserted into the hole. A force and moment applied to the peg whose values lie within the parallelogram shaped region will slide the peg into the hole regardless of the direction of tilt of the peg, or whether the peg is in one or two-point contact with the hole.

The existence of such a "sliding region" for arbitrary one and two-point contacts between the peg and hole is central to the RCC's ability to perform insertions reliably. Specifically, the strategy implicit in the design of the RCC is to ensure that no configuration that could cause the assembly to terminate will be encountered.

In terms of the diagram in Figure 1, the lines defining the boundaries of the sliding region correspond to the sliding constraints for each of the six possible contact configurations the peg encounters inside the hole. Because the intersection of the constraints for all possible configurations exists, an applied force and moment, or set of forces and moments, chosen from that intersection region will succeed in sliding the peg into the hole without jamming. We will see in the next section that it is

CH2750-8/89/0000/0472$01.00 © 1989 IEEE

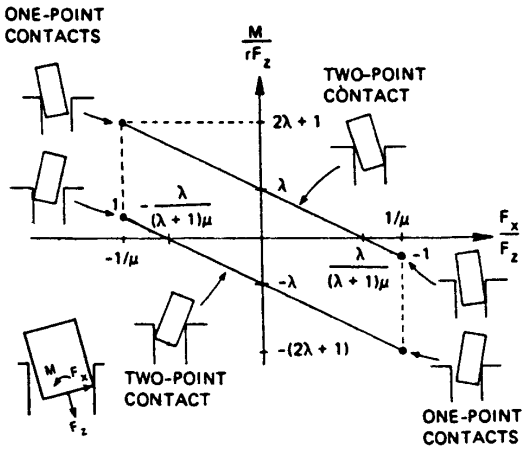

Figure 1: Jamming Diagram for the RCC (from Whitney [8])

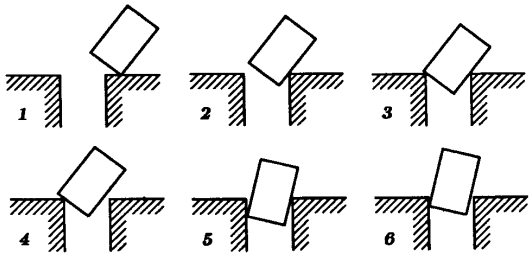

Figure 2: Some Contact Configurations for the Planar Peg and Hole

the presence of chamfers on the hole that allows such a solution to be found.

The Planar Peg and Hole Without Chamfers

We begin by considering the set of possible configurations of contact between a planar peg and a hole without chamfers. If we restrict ourselves to considering only point contacts there are 12 possible cases, of which 6 are shown in Figure 2.[1]

Next we follow the approach used by Whitney to examine the force interactions between the peg and hole. Figure 3 shows a force and moment applied to the peg and the corresponding reaction forces at the points of contact with the hole for configuration 5. In our models we assume the parts to be infinitely rigid and massless, and we use the dry Coulomb model to represent friction. The applied force is represented as a vector F applied to the top of the peg at an angle α with respect to the axis of the peg, and the applied moment M has the sense shown. The resulting equilibrium relations expressed in the coordinates

[1]The remaining six configurations are similar to those shown, but with the peg tilted in the opposite sense.

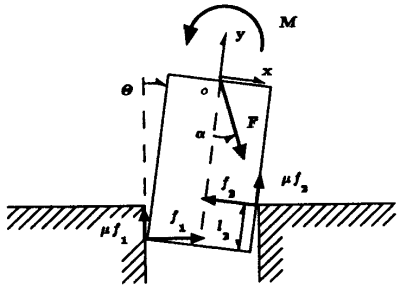

Figure 3: Quasi-Static Equilibrium for Configuration 5

of the peg are:

$$\sum F_x = 0 \;=\; F\sin\alpha + f_1\cos\theta - \mu f_1\sin\theta - f_2 \qquad (1)$$

$$\sum F_y = 0 \;=\; -F\cos\alpha + f_1\sin\theta + \mu f_1\cos\theta + \mu f_2 \qquad (2)$$

$$\sum M_o = 0 \;=\; M + \mu f_2 d + f_2 l_2 - F(\frac{d}{2})\cos\alpha - FL\sin\alpha \qquad (3)$$

The above equations assume conditions of quasi-static equilibrium with the peg in a state of impending motion relative to the hole. We may reformulate the above equations into inequalities by introducing a small perturbation δ to the tangential component of each reaction force. Specifically, if we replace each μf_i with $\mu f_i + \delta$, the resulting expressions will determine the applied force and moment necessary to balance this extra tangential component of the reaction force. Solving for $\delta \geq 0$ the resulting inequalities will specify the desired sense of sliding motion.

To maintain the conditions of two-point contact we require f_1 and $f_2 \geq 0$. Solutions for either f_1 or $f_2 = 0$ correspond to one-point contact. Next we solve the resulting expressions for δ, f_1 and f_2 all greater than or equal to zero, and include the kinematic constraint for the insertion depth l_2 in terms of the angle of tilt of the peg θ as:

$$l_2 = \frac{D - d\cos\theta}{\sin\theta} \qquad (4)$$

The result is:

$$\arctan\left(\frac{\mu\sin\theta - \cos\theta}{\mu\cos\theta + \sin\theta}\right) \leq \alpha \leq \arctan\left(\frac{1}{\mu}\right) \qquad (5)$$

and:

$$\frac{M}{F} \geq \sin\alpha\left[L - \frac{D(\mu\cos\theta + \sin\theta) + d(\frac{\mu^2-1}{2}\sin 2\theta - \mu\cos 2\theta)}{1 - (\mu\sin\theta - \cos\theta)^2}\right] + \cos\alpha\left[\frac{d + D(\mu\sin\theta - \cos\theta)}{1 - (\mu\sin\theta - \cos\theta)^2} - \frac{d}{2}\right] \qquad (6)$$

The above inequalities determine the force F, the angle α at which the force is applied to the peg, and the moment M necessary to achieve sliding in configuration 5. We can derive similar expressions for the analogous configuration with the peg tilted in the opposite sense, which we will term configuration 5′.

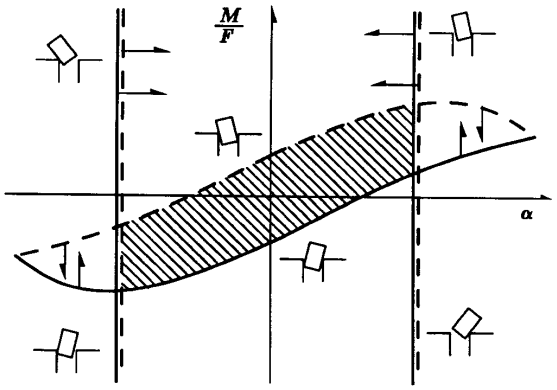

Figure 4: Applied Force & Moment Constraint Space, configs. 5 & 5′

Similar to the analysis for the RCC, we may represent the constraints on the applied force and moment for configurations 5 and 5′ graphically in a two dimensional space as shown in Figure 4. Here we have chosen the axes to be the ratio of the applied moment M to the applied force F, and the angle of the applied force α with respect to the axis of the peg. As was true for the chamfered peg and hole, there is an intersection region (shaded) representing values of the applied force and moment that will slide the peg into the hole for either configuration 5 or 5′.

Since there are no chamfers to ensure that two-point contact occurs only after the peg enters the hole, another likely configuration to be encountered is configuration 3 (or 3′), shown in Figure 5. As before, we may express the quasi-static equilibrium relations as:

$$\sum F_x = 0 \quad = \quad F\sin\alpha - \mu f_1 - f_2 \tag{7}$$

$$\sum F_y = 0 \quad = \quad -F\cos\alpha + f_1 - \mu f_2 \tag{8}$$

$$\sum M_o = 0 \quad = \quad M - \mu f_1 L - f_1(\frac{d}{2} - l_1) - \mu f_2 \frac{d}{2} - f_2(L - l_2) \tag{9}$$

The resulting constraint expressions for configuration 3 are:

$$\alpha \geq \arctan\left(-\frac{1}{\mu}\right) \tag{10}$$

$$\alpha \geq \arctan(\mu) \tag{11}$$

$$\frac{M}{F} \geq \sin\alpha\left[L + D\frac{\mu\cos\theta - \sin\theta}{\mu^2+1}\right] + \cos\alpha\left[-\frac{d}{2} + D\frac{\cos\theta + \mu\sin\theta}{\mu^2+1}\right] \tag{12}$$

As was done for configurations 5 and 5′ we represent the sliding constraint inequalities graphically as shown in Figure 6. Unlike the figure for configurations 5 and 5′, however, there is no intersection region valid for both tilts of the peg. In other words, there is no single force-moment combination that will

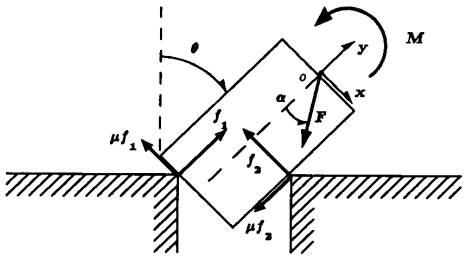

Figure 5: Quasi-Static Equilibrium for Configuration 3

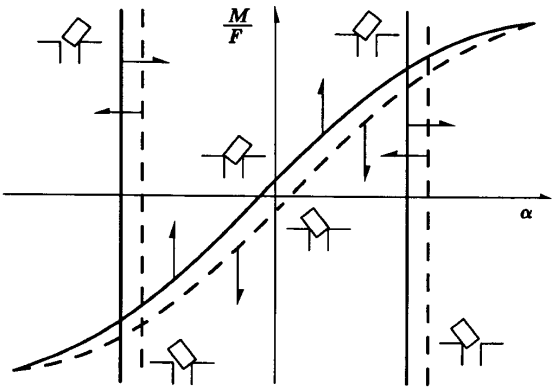

Figure 6: Applied Force & Moment Constraint Space, configs. 3 & 3′

slide the peg into the hole if the peg is allowed to tilt in either direction.

Since we cannot reliably predict in which way the peg will be tilted when it contacts the edge of the hole, a strategy based on applying an arbitrary force suitable for either configuration will not succeed. If the hole had chamfers, of course, we would not face this dilemma since the presence of chamfers significantly increases the likelyhood that the peg will enter the hole before encountering a two-point contact configuration, where a solution is known to exist. Clearly we must re-examine our assumption that a successful assembly strategy must satisfy the constraints imposed by all possible configurations.

Constraining the Configurations: A Solution

Since we cannot find a solution valid for all contact configurations of the peg and hole, a logical step would be to constrain the assembly to some allowable subset of configurations for which a solution can be found. Specifically, by eliminating the ambiguous initial condition of allowing the peg to be tilted in either direction, we may relax the sliding constraints on the applied force and moment. For example, let us assume the peg to be tilted initially in the positive θ direction, corresponding to configuration 3. We further assume that we may restrict the motion of the peg such that the only other configuration that will be encountered is configuration 5. If we can ensure that our

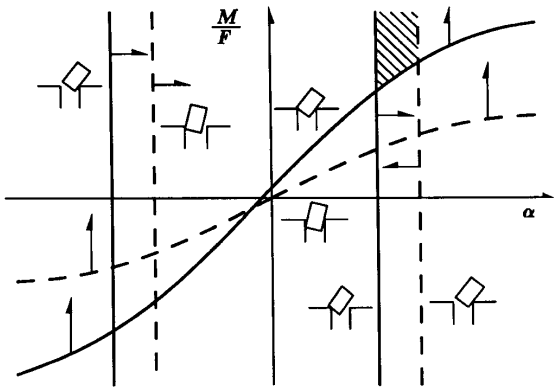

Figure 7: Applied Force & Moment Constraint Space, configs. 3 & 5 at θ_c

strategy meets these new constraints, we may ignore the sliding constraints for configurations 3′ and 5′. The critical point in this strategy occurs at the transition between configurations 3 and 5, i.e. when the outside corner of the peg just crosses the top edge of the hole. The angle at which this transition occurs is given by:

$$\theta_c = \arccos\left(\frac{d}{D}\right) \tag{13}$$

When we plot the sliding constraints for both configurations 3 and 5 at θ_c, we obtain the plot shown in Figure 7. The shaded intersection region represents the set of applied forces and moments that will slide the peg into the hole from an initially tilted configuration. Therefore, to guarantee successful insertion we will constrain the peg to slide in two-point contact from configuration 3 to configuration 5, avoiding other configurations that may cause the insertion to fail.

In summary, a successful strategy for the insertion of a planar peg into a hole without the aid of chamfers is to tilt the peg relative to the hole and place the bottom corner of the peg into the hole. In addition to eliminating the constraints associated with the ambiguity of the direction of tilt of the peg, the precision required to start the assembly in this configuration is reduced [3]. Once the peg is in contact with the hole in a tilted configuration (config. 3), the peg may be rotated while maintaining sliding contact with the hole by the application of the appropriate force and moment as determined from Figure 7. At some point during this rotation, given by θ_c, the opposite corner of the peg will clear the top edge of the hole and the peg will slide into the hole (config. 5) without jamming. Because the sliding regions are not sensitive to the position of the peg in any one configuration, the resulting strategy is not sensitive to positional uncertainty.

Extending to Three Dimensions

The rotational symmetry of cylindrically shaped parts allows strategies for such parts to be developed using planar models similar to the one described above. Since many parts do not exhibit rotational symmetry, and therefore do not lend themselves to planar analysis, it is necessary to extend the above analysis

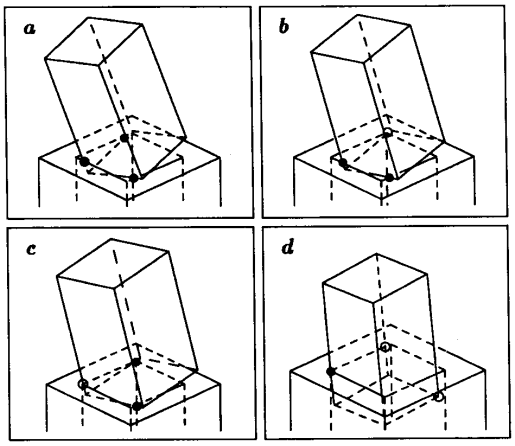

Figure 8: A Suitable Subset of Configurations for the Peg and Hole

to three dimensions. In this section we will briefly examine such an extension.

One example of a non-axisymmetric three-dimensional assembly is the rectangular peg and hole shown in Figure 8. As for the planar peg and hole, we begin by enumerating the set of possible contact configurations between the peg and hole, assuming only point contacts.[2] Expanding over the set of contacts results in 1060 possible configurations between the peg and the hole [1].

As we saw in the previous section, we must select an appropriate set of configurations through which the parts may pass to reliably perform an assembly. However, given 1060 possible configurations for even such simple parts, it would be impractical to completely model and analyze each and every configuration in order to find a few with which to characterize an assembly path. To overcome this, we adopt a set of heuristics to aid in finding suitable configurations.

From the results of the previous section we found that tilting the peg relative to the hole simplifies the problem of initially positioning the peg. For the three-dimensional rectangular case we select an initial configuration with the peg tilted about all three axes as shown in Figure 8a. Here the contacts are between a side edge and two adjacent bottom edges of the peg and three adjacent top edges of the hole.

We know that the degree of positional uncertainty in a system is proportional to the degrees of freedom of that system. Therefore, choosing a series of configurations that sequentially reduce the number of degrees of freedom helps to reduce the degree of positional uncertainty present in a system. To improve the robustness of our strategy in the presence of uncertainty, we wish to select a set of configurations which are reachable via sliding motion from the initial configuration **a** and will reduce the degrees of freedom of the peg. One such configuration is shown in Figure 8 **b**. Here, one of the bottom edges of the peg that was in contact with a top edge of the hole has slid into

[2]The point contacts are of the form peg-edge/hole-edge or peg-vertex/hole-face. See [1] section 3.2.2.

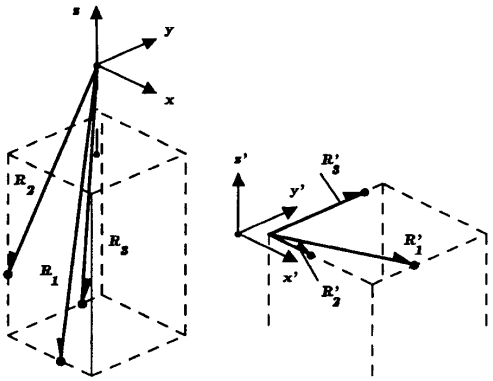

Figure 9: Contact Vectors for Configuration a

contact with the adjacent corner of the hole (hollow circle). The degrees of freedom of the peg have been reduced from 3 in configuration a to 2 in configuration b.

Configuration c subsequently reduces the degrees of freedom of the peg from 2 to 1. With only 1 degree of freedom remaining in configuration c the next configuration will be achieved when one of the three remaining corners of the peg outside of the hole clears the top edge and the peg enters the hole. A peg with a nearly square cross section will end up in configuration d as shown in Figure 8d.

Having chosen a set of configurations through which the peg is to pass during insertion, we begin the analysis by determining the kinematic constraints between the peg and hole for each of the above configurations. Figure 9 shows the points of contact between the peg and the hole for configuration a. The contact vectors $\vec{R}_1$, $\vec{R}_2$, and $\vec{R}_3$ for the peg, and $\vec{R_1}'$, $\vec{R_2}'$, and $\vec{R_3}'$ for the hole, specify the locations of the points of contact relative to the coordinate frames of the peg and hole respectively. The kinematic constraints between the peg and hole for configuration a may then be determined by constraining the corresponding pairs of contact points for both the peg and the hole to simultaneously remain on their respective edges.

Since we have modeled only configurations a through d, we must constrain the direction in which the peg slides to guarantee we encounter only those configurations. To do this we specify a nominal position of the peg P_i, within an associated error bound ϵ, in a given configuration. We then specify a range of goal positions P_{goal} within the subsequent target configuration. The range of directions of motion that will reach a point within P_{goal} are then determined by constructing a velocity error cone from P_i to P_{goal}.

After specifying the set of configurations a through d and determinging the range of sliding motions necessary to reach only these configurations, we derive the expressions for the corresponding quasi-static force and moment equilibrium in each configuration. With respect to the coordinate frame of the peg these are of the form:

$$\sum \vec{F} = 0 \quad = \quad \vec{F}_{ext} + \sum_{i=1}^{n} (f_i \vec{n}_i - \mu f_i \vec{v}_i - \delta \vec{v}_i) \qquad (14)$$

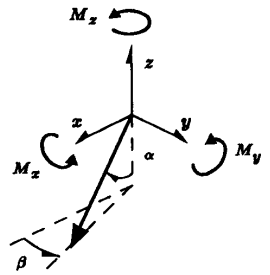

Figure 10: Representation of Applied Force and Moment

$$\sum \vec{M} = 0 \quad = \quad \vec{M}_{ext} + \sum_{i=1}^{n} ((\vec{R}_i \times f_i \vec{n}_i) - (\vec{R}_i \times \mu f_i \vec{v}_i) - (\vec{R}_i \times \delta \vec{v}_i)) \qquad (15)$$

where $\vec{n}_i$ and $\vec{v}_i$ are the unit normal and unit velocity vectors, respectively, of the ith contact point between the peg and hole. Unlike the planar case, the resulting constraint relations are too large and complex to be solved manually and were therefore solved symbolically on a computer using MACSYMA.

We may represent the force to be applied to the peg in spherical coordinates as a magnitude F and two angles, α and β, and the applied moment as three orthogonal components (M_x, M_y, M_z) as shown in Figure 10. As in the planar case we may normalize the components of the moment with respect to the magnitude of the force F, resulting in five applied force-moment parameters $(\frac{M_x}{F}, \frac{M_y}{F}, \frac{M_z}{F}, \alpha, \beta)$.

For visualization purposes we may represent the constraint expressions for sliding as surfaces in 3 three-dimensional subspaces whose axes are:

$$(\frac{M_x}{F}, \alpha, \beta), (\frac{M_y}{F}, \alpha, \beta), (\frac{M_z}{F}, \alpha, \beta)$$

The resulting constraint surfaces for configuration a are shown in Figure 11. As in the planar case we intersect the sliding constraints for each configuration to determine the set of applied forces and moments that will satisfy the above constraints.

The major limitation of the above approach to finding suitable applied forces and moments is that we are not guaranteed to find a single intersection region in force-moment space valid for the entire set of configurations chosen. This would indicate that the configurations chosen may not all be reachable reliably by the application of a single force and moment vector.

Lacking an intersection region in force-moment space we are left with two possible courses of action. One is to re-examine the chosen configurations and select another set. The other option is to abandon a strategy that relies on only a single force and moment to complete the entire assembly. In the latter case, we must determine in what configuration the peg will become jammed and use that configuration as the starting point for a subsequent force and moment to be applied.

The second option is undesirable because it requires multiple forces and moments to be applied, and that we be able to determine when the assembly has jammed so that the next force and moment may be applied. Such a multi-step strategy would all but rule out the possibility of implementing the strategy with a passive, i.e. sensorless, device.

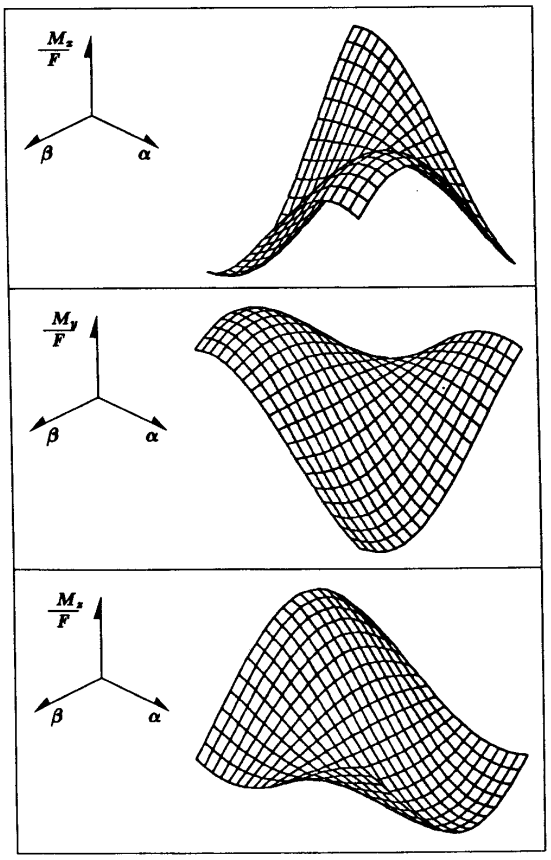

Figure 11: Sliding Constraints for Config. a.

Conclusions

We have seen from the analysis of the insertion of a planar peg into a chamferless hole that there are cases where an assembly may not be reliably carried out if the contact configurations between parts are not constrained. In such cases it is necessary to a priori specify the configurations through which the assembly must pass, and guarantee that only those configurations are encountered.

From the analysis for the insertion of a three dimensional rectangular peg into a chamferless hole we have seen that, for moderately complex assemblies involving many possible configurations, the specification of a set of configurations through which parts must pass is considerably more difficult than for the planar case. However, by considering only a subset of the possible configurations chosen on the basis of a set of heuristics, successful assembly strategies can be generated.

The assembly strategies developed for the previous two examples were implemented and tested. In the planar case a passive mechanism was developed that successfully performed chamferless insertion of a peg into a hole. For the three dimensional peg and hole example, a robot operating under force control was used.

Acknowledgments

The research described in this paper was performed at the Massachusetts Institute of Technology Artificial Intelligence Laboratory. This work was funded by the Office of Naval Research under the University Research Initative Program through contract N00014-86-K-0685. Additional support was provided by an NSF Presidential Young Investigator Award (Lozano-Pérez).

References

[1] **M. E. Caine**, "Chamferless Assembly of Rectangular Parts in Two and Three Dimensions", S.M. Thesis, Department of Mechanical Engineering, Massachusetts Institute of Technology, June 1985.

[2] **M. A. Erdmann**, "On Motion Planning with Uncertainty", Artificial Intelligence Laboratory, Massachusetts Institute of Technology, Technical Report 810, May 1984.

[3] **H. Inoue**, "Force Feedback in Precise Assembly Tasks", Artificial Intelligence Laboratory, Massachusetts Institute of Technology, AI Memo-308, Aug. 1974 (Reprinted in Winston, P. H., and Brown, R. H., eds., *Artificial Intelligence: An MIT Perspective*, MIT Press, 1979).

[4] **T. Lozano-Pérez, M. T. Mason, R. H. Taylor**, "Automatic Synthesis of Fine-Motion Strategies for Robots", *Proceedings, International Symposium of Robotics Research*, Bretton Woods, NH, MIT Press, Sept. 1984.

[5] **M. T. Mason**, "Compliance and Force Control for Computer Controlled Manipulators", *IEEE Transactions on Systems, Man, and Cybernetics*, Vol. SMC-11, No. 6, June 1981 (Reprinted in Brady, M. et al., eds., *Robot Motion*, MIT Press, 1983).

[6] **M. S. Ohwovoriole, B. Roth**, "A Theory of Parts Mating for Assembly Automation", *Proceedings of the Robot and Man Symposium 81*, Warsaw, Poland, Sept. 1981.

[7] **S. N. Simunovic**, "An Information Approach to Parts Mating", Ph.D. Thesis, Department of Mechanical Engineering, Massachusetts Institute of Technology, April 1979.

[8] **D. E. Whitney**, "Quasi-Static Assembly of Compliantly Supported Rigid Parts", *Journal of Dynamic Systems, Measurement, and Control*, Vol. 104, March 1982, pp. 65-77.